IEEE Transactions on Nuclear Science, Vol. NS-32, No. 5, October 1985

NONLINEAR EFFECTS OF FOCUSING BARS USED IN THE EXTRACTION SYSTEMS OF SUPERCONDUCTING CYCLOTRONS*

M.M. GORDON and V. TAIVASSALO

National Superconducting Cyclotron Laboratory, Michigan State University, East Lansing, MI 48824

Abstract

Sets of rectangular iron bars are used in combination with electostatic deflectors to focus and bend the beam along its path out of the cyclotron field. Since the design of this system was based on conventional orbit computations that include only linear vertical motion, additional studies have been undertaken to evaluate the nonlinear effects on the phase space of the extracted beam. These studies are carried out with a special orbit code that uses exact equations of motion, and treats the main cyclotron field correctly to fourth order in z. In addition, the rectangular focusing bars are assumed to be uniformly magnetized so that the resultant field can be calculated exactly on and off the median plane using simple formulas. Some preliminary results from this orbit code are presented here that show how the final radial and vertical phase space properties depend on the initial emittance values, and how they are changed by possible small displacements of the focusing bars.

1. Introduction

The final design calculations for the extraction system now used in our K500 cyclotron were carried out by Fabrici, Johnson and Resmini,[1] and the general properties of this system are described in their paper. Starting at $\theta=-23^{\circ}$ and r=26.5 in., the beam first passes through two electrostatic deflectors and then through eight focusing bars which provide essential radial focusing together with substantial bending capability. When the beam completes this part of the deflection process, it has just reached the outer radius of the superconducting coils, r=36 in.

Nonlinear effects should be important here first of all because of the rapid fall-off of the main magnetic field in the extraction region, and second because the effectiveness of the focusing bars requires that their own magnet gap be very small. These effects will, of course, manifest themselves through increases in the emittance values of the extracted beam.

During the past year, all of the orbit codes used to carry out design calculations like those described above have been modified to incorporate more accurate formulas for the fields of the focusing bars. These formulas are based on the H field produced by a uniformly charged rectangular sheet parallel to the median plane, since this field can be calculated exactly at any point from simple analytical formulas. By using two such sheets at $+z_o$ and $-z_o$ with equal and opposite charges, one can represent a rectangular iron bar which is uniformly magnetized in the z direction.

The eight focusing bars used in the extraction system each consist of three such iron bars. Our revised programs now compute the resultant field of all these bars (plus two compensating bars) by superimposing the fields of the individual bars.

The new orbit code is an extension of the "Z-4 Spiral Gap Code" which was first developed in 1978.[2] In this code, the median plane field data are processed so as to allow the calculation of all components of the main field correctly to fourth order in z. The code then adds to this field the "exact" fields produced by all of the focusing bars and compensating bars. This combined field is computed as needed along the orbit through the extraction system. This code can also be used for pre-extraction calculations, but these will not concern us here.

2. Initial Conditions

The main field used in these studies was designed to accelerate C^{4+} ions to a final energy of about 30 MeV/A. All of the orbits considered here were started at $\theta=-23^{\circ}$, at the entrance of the first deflector, and with the nominal extraction energy E=29.9 MeV/A, corresponding to $\nu_r=0.81$ and $\nu_z=0.94$. These orbits were then computed to $\theta=300^{\circ}$, just beyond the last focusing bar, M8. The central ray was computed first, with the radial positions of the eight focusing bars being adjusted so that this trajectory matched as well as possible the prescribed shape over the given θ range.

In order to obtain a broad range of orbit data, 25 sets of displaced rays were computed with initial (x,p_x) and (z,p_z) points on a pair of eigenellipses having initial emittance values from 0 to 20 mm-mrad, in steps of 5 mm-mrad. One such pair with 5 mm-mrad radially and 10mm-mrad vertically is shown in Fig. 1, together with the 8×16 pairs of initial conditions used in this case. Because of median plane symmetry, only half of the (z,p_z) values are actually used.

3. Final Emittance Values

In obtaining the final emitttance values at $\theta=300^{\circ}$, all possible ellipses were considered which completely contained the (x,p_x) or (z,p_z) points in a given set, and the one having the smallest area was determined by a linear programming subroutine. Denoting this area by ε', the final radial or vertical emittance was then defined to be

$$\varepsilon = \varepsilon_o + \tfrac{1}{2}(\varepsilon' - \varepsilon_o),$$

where ε_o is the initial value. This somewhat arbitrary definition was chosen because the number of points to be considered varied between 8 and 64, so that the usual 90% rule could not be applied consistently.

MSU-85-257

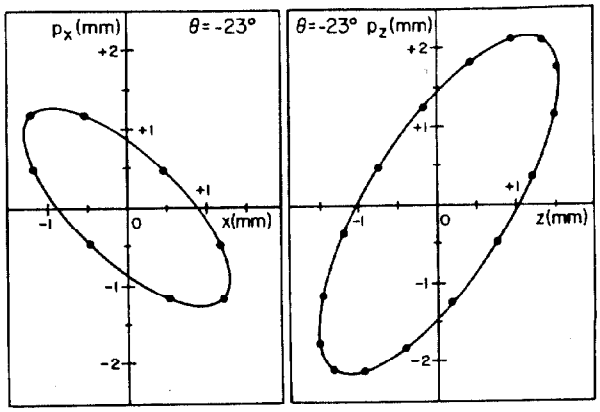

Fig. 1 Initial conditions for Figs. 4 and 5. The 8 16 pairs of points are for initial radial (left) and vertical (right) emittances of 5 and 10 mm-mrad, respectively. Note that 1.0 mm = 1.4 mrad for p_x or p_x in our units.

0018-9499/85/1000-2447$01.00© 1985 IEEE

Although the results obtained for the final emittances can be displayed in different ways, the plots shown in Figs. 2 and 3 serve to give greater emphasis to the coupling effects. That is, Fig. 2 shows the final radial versus the initial vertical emittance, while Fig. 3 shows the final vertical versus the initial radial emittance.

These curves indicate that for initial values between 0 and 10 (mm-mrad), the rise in ε_x and ε_z is almost linear, with increases of about 10% and 20%, respectively. They also show that as the initial values increase from 10 to 20, the curves continue to rise, but their shapes differ significantly.

The data also show that if the initial vertical emittance is twice the radial one, then the percentage increase in both is about the same. That is, for $(\varepsilon_{xo}, \varepsilon_{zo}) = (5,10)$ and $(10,20)$, the increases are: $(\delta\varepsilon_x, \delta\varepsilon_z) = (12\%, 9\%)$ and $(21\%, 23\%)$.

On the other hand, if the initial emittances are equal, the increase in the final vertical emittance is about twice that for the radial one. That is, for $\varepsilon_{xo} = \varepsilon_{zo} = 10$, 15, and 20, respectively, the increases are $(\delta\varepsilon_x, \delta\varepsilon_z) = (10\%, 18\%)$, $(14\%, 29\%)$, and $(18\%, 42\%)$.

4. Phase-Space Distortions

The final emittance values give only a rough idea of the nonlinear effects, and we consider now the distribution of (x,p_x) and (z,p_z) points at $\theta = 300^\circ$ obtained for one set of orbits, namely those whose initial conditions are shown in Fig. 1. This set with $\varepsilon_{xo} = 5$ and $\varepsilon_{zo} = 10$ mm-mrad, represents approximately the values expected for the K500 cyclotron when operating without phase selection.

The radial and vertical phase-space diagrams presented in Fig. 4 show several different plots for comparison. First, the two solid ellipses demonstrate the results that would be obtained if the motion were completely linear. Next to each ellipse are 8 plotted points which give the actual values obtained for (x,p_x) when $\varepsilon_{zo} = 0$ (i.e., for median plane motion) and for (z,p_z) when $\varepsilon_{xo} = 0$. Evidently, the deviations of these points from the corresponding ellipses are rather small, which indicates that in this case at least, the nonlinearities in the motion are relatively weak.

Next, Fig. 4 shows in each case 8 sets of small closed curves which reveal how the 8 points described above evolve when the initial emittances are changed to $\varepsilon_{xo}=5$ and $\varepsilon_{zo}=10$, that is, with the coupling effects totally present. In addition, a ninth curve is shown near $(x,p_x) = 0$ which indicates the corresponding evolution of the central ray ($\varepsilon_{xo}=0$) when the vertical motion is included. Finally, the broken curve enclosing all these points is in each case the ellipse having the minimum area ε' described in Sec. 3.

In the radial phase-space diagram, it is evident that the 9 small curves lack any symmetry and vary considerable in size and shape. Moreover, most of these curves do not enclose the 9 points (including the central ray) from which they evolved.

In the phase-space diagram for the z motion, the corresponding 8 curves also exhibit considerable variation in size and shape. Indeed, at least two of these curves have actually folded over into shapes like a figure 8. Comparing these curves with those for the radial motion, we find that the average size here is greater by more than a factor of 2, the ratio of initial emittances.

With regard to the source of the distortions

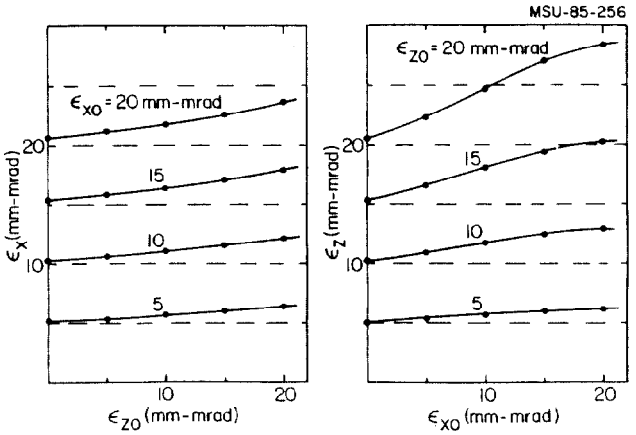

Fig. 2 (left) Final radial vs. initial vertical emittances.
Fig. 3 (right) Final vertical vs. initial radial emittances.

shown in these diagrams, we note that the code can be run with either the main field or the focusing bar field completely linear in z. The results of such runs show that the focusing bars are responsible for about 70% to 90% of the effects observed here.

5. Displaced Focusing Bars

The radial positions of the eight focusing bars are adjusted empirically (along with other parameters) in order to optimize the beam current extracted from the cyclotron. The position of the beam's central ray is somewhat uncertain, and could in practice deviate from the symmetry axis by as much as ±0.1 in.

In order to investigate the effects of such deviations, we shifted the radial position of M1 by different amounts and then shifted the remaining focusing bars so as to restore the value of (r,p_r) for the central ray at $\theta = 300^\circ$. Such displacements will, of course, not affect the trajectory beyond this θ, but they will change the focusing condition of the beam.

We consider here only the results obtained when M1 was displaced by $\delta r = +50$ and -50 mils. The resultant shifts of all 8 focusing bars in these two cases are listed respectively in the top two and bottom two rows of the Table below. The values of δr give the radial shifts of the focusing bars themselves, while $\delta\bar{X}$ gives the average displacement of the central ray from the symmetry axis for each focusing bar. In addition, the center row gives for comparison the $\delta\bar{X}$ values for the original central ray. All values are in mils and 39 mils = 1mm.

	M1	M2	M3	M4	M5	M6	M7	M8
$\delta r(+)$	+50	-30	-20	-50	-50	-60	+110	+70
$\delta\bar{X}(+)$	-40	+96	+98	+122	+107	+87	-99	-70
$\delta\bar{X}(0)$	+6	-9	-11	-15	-7	-18	-10	-8
$\delta\bar{X}(-)$	+53	-115	-118	-149	-116	-115	+90	+67
$\delta r(-)$	-50	+30	+20	+50	+50	+60	-110	-70

Comparing values in the top and bottom two rows, we find that even though the δr values are perfectly symmetric, the $\delta\bar{X}$ values are not. But most of the differences are small with the largest being about ±15%. Of greater importance are the magnitudes of $\delta\bar{X}$ which are obviously much larger than for the original central ray. Such deviations should, of course, increase the nonlinear effects.

Consider first the changes in final emittance

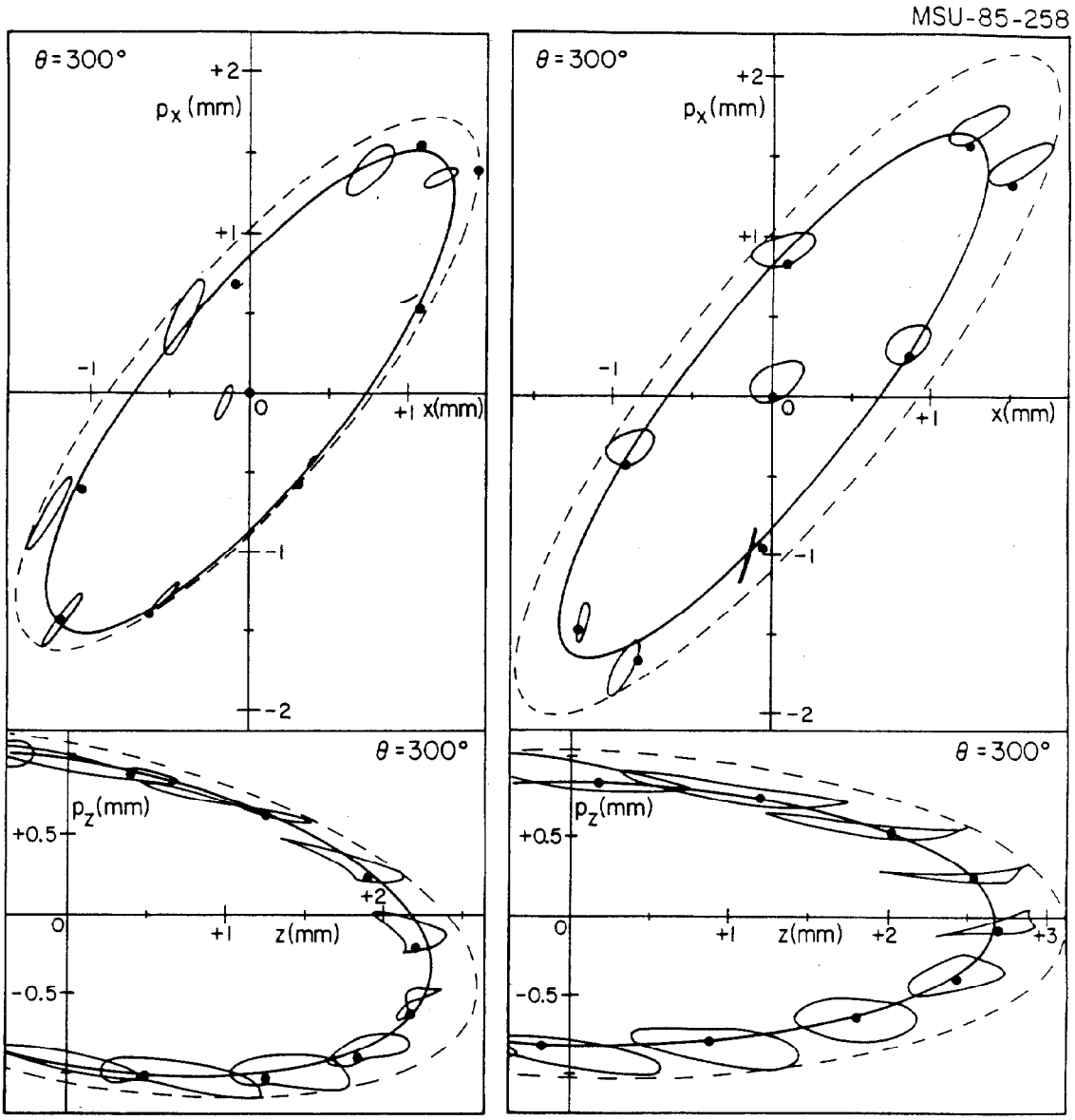

Fig. 4 (left) Diagrams for final radial (top) and vertical (bottom) phase-space distributions described in Sec. 4.

Fig. 5 (right) Corresponding results for one case of displaced focusing bars described in Sec. 5. (See Fig. 1)

values. We find that for displacements of M1 by δr = 0, +50, and -50 mils, respectively, the final emittances are: ε_x = 5.62, 6.51, and 5.93, while ε_z = 10.93, 12.26, and 11.78 mm-mrad. Thus, the largest increase is about 16%, which is reasonably tolerable.

The effects of the displacements on the radial and vertical phase space are shown in Fig. 5 for the case where M1 was shifted by +50 mils. For ease of comparison, this figure is placed side by side with Fig. 4, and is drawn with the same layout and scales. One can therefore see immediately the kinds of changes that may occur when the focusing bars are displaced.

With regard to actual measurements on the K500 cyclotron, the available data so far are very sparse. One set of measurements on the external beam yielded ε_x = 8 and ε_z = 17 mm-mrad, but the interpretation is rather uncertain because the measurements also indicated that the beam contained two different energy groups. These results were obtained some time ago and although other indicators show that the beam properties have generally improved in the meantime, no further emittance measurements have as yet been carried out. Such measurements, in combination with orbit calculations, will be useful in evaluating nonlinear effects.

* This work supported by the National Science Foundation under Grant No. PHY-83-12245

References

1. E. Fabrici, D. Johnson and F.G. Resmini, Nucl. Instr. and Meth. 184,301(1981).
2. M.M. Gordon, Nucl. Instr. and Meth. 169,327(1980).